Published in final edited form as:
Cell Host Microbe. 2010 April 22; 7(4): 314–323. doi:10.1016/j.chom.2010.03.005.

Structural basis of HIV-1 tethering to membranes by the Bst2/tetherin ectodomain

Andreas Hinz[1,6], **Nolwenn Miguet**[1,6], **Ganesh Natrajan**[1], **Yoshiko Usami**[2], **Hikaru Yamanaka**[2], **Patricia Renesto**[1], **Bettina Hartlieb**[1], **Andrew A. McCarthy**[1,3], **Jean-Pierre Simorre**[4], **Heinrich Gottlinger**[2], and **Winfried Weissenhorn**[1,5]

[1]Unit of Virus Host Cell Interactions (UVHCI) UMI 3265 Université Joseph Fourier-EMBL-CNRS, 6 rue Jules Horowitz 38042 Grenoble, France

[2]Program in Gene Function and Expression, Program in Molecular Medicine, University of Massachusetts Medical School, Worcester, MA 01605, USA

[3]EMBL, 6 rue Jules Horowitz 38042 Grenoble, France

[4]Institut de Biologie Structurale Jean-Pierre Ebel, UMR 5075 CEA-CNRS-UJF, 41 rue Jules Horowitz, 38027 Grenoble Cedex 01, France

SUMMARY

The restriction factor Bst2/tetherin contains two membrane anchors which are employed to retain some enveloped viruses including HIV-1 tethered to the plasma membrane in the absence of virus encoded antagonists. The 2.77 Å crystal structure of the extracellular core presented here reveals a parallel 90 Å long disulfide linked coiled-coil domain while the complete extracellular domain forms an extended 170 Å long rod-like structure based on small angle X-ray scattering data. Mutagenesis analyses indicate that both the coiled-coil and the N-terminal region are required for retention of HIV-1, suggesting that the elongated structure can function as a molecular ruler to bridge long distances. The structure reveals substantial irregularities and instabilities throughout the coiled-coil, which contribute to its low stability in the absence of disulfide bonds. We propose that the irregular coiled-coil provides conformational flexibility and ensures that Bst2/tetherin anchoring in the plasma and the newly formed virus membrane do not interfere with budding.

INTRODUCTION

Enveloped viruses rely on host cell factors to complete their life cycle. These factors act as positive or negative regulators, such as restriction factors, that often limit replication to a narrow range of hosts and cell types (Malim and Emerman, 2008). Whilst restriction factors are inducible by interferon (INF) and thus constitute a first line of innate immune defense, viral proteins that render cells permissive for infection can counteract this mechanism. Certain cell types such as HeLa cells require the expression of the HIV-1 cofactor Vpu for particle release (Gottlinger et al., 1993; Klimkait et al., 1990; Strebel et al., 1989; Terwilliger et al., 1989) although replication occurs independently of Vpu in other cells

[5]Corresponding author: weissenhorn@embl.fr, Tel: 33-476-207281, Fax: 33-476-209400.
[6]These authors contributed equally

(Gramberg et al., 2009; Strebel et al., 2009). This restriction was attributed to the presence or absence of Bst2, also known as tetherin (or CD317 and HM1.24) (Neil et al., 2008; Van Damme et al., 2008). Bst2/tetherin was originally linked to B cell development and shown to be a marker of multiple myeloma cells (Goto et al., 1994; Masuyama et al., 2009; Ohtomo et al., 1999). Its expression is induced by interferon-α (Kawai et al., 2008) and INF-α activation leads to HIV-1 retention at the plasma membrane in the absence of Vpu (Neil et al., 2007).

Bst2/tetherin is a type II transmembrane protein, composed of a small cytosolic domain, an N-terminal transmembrane region (TMR) and an extracellular domain modified by a second membrane anchor, a C-terminal glycosyl-phosphatidylinositol (GPI) (Kupzig et al., 2003). Bst2/tetherin resides in lipid rafts at the cell surface and membranes of the trans Golgi network (TGN) (Kupzig et al., 2003). In HIV-1 infected cells tetherin is retained in the TGN by Vpu (Neil et al., 2008; Van Damme et al., 2008) and targeted for endocytosis and degradation (Douglas et al., 2009; Goffinet et al., 2009;Harila et al., 2007; Mangeat et al., 2009; Mitchell et al., 2009). Although it should be noted that enhancement of virus release by Vpu does not depend on down-regulation or degradation of tetherin in some specific cell lines (Miyagi et al., 2009).

Inhibition of tetherin by Vpu is species-specific and suggests that Vpu's activity evolved to specifically counteract human tetherin (Goffinet et al., 2009; Gupta et al., 2009; Jia et al., 2009; Sauter et al., 2009). Vpu-mediated tetherin retention requires the TMR of tetherin (McNatt et al., 2009; Rong et al., 2009) or all structural domains (Goffinet et al., 2009) and the TMR and cytosolic domain of Vpu (Van Damme et al., 2008).

The anti-viral function of tetherin is not limited to HIV-1 or other retroviruses (Jouvenet et al., 2009; Zhang et al., 2009) as it also restricts release of filoviruses (Jouvenet et al., 2009; Kaletsky et al., 2009), arena viruses (Sakuma et al., 2009a) and KSHV (Bartee et al., 2006) in the absence of their respective antagonists.

Tetherin has been suggested to span both the cellular and viral membranes (Neil et al., 2008) based on its double membrane-anchored topology (Kupzig et al., 2003), its ability to form disulfide-linked dimers (Ohtomo et al., 1999) and the presence of a predicted coiled-coil sequence in the extracellular domain. Tetherin is present in the viral membrane as a homodimer and either TMR or the GPI anchor must be inserted into virion envelopes for successful retention (Perez-Caballero et al., 2009). Furthermore disulfide-cross-linking via any of the three cysteines and the spacer function of the coiled-coil are necessary for anti-viral activity (Andrew et al., 2009; Perez-Caballero et al., 2009).

Here we present the crystal structure of a core fragment of human tetherin, which forms a 90 Å long parallel coiled-coil. The complete extracellular region adopts a ~ 170 Å long bent rod-like structure based on small angle X-ray scattering analysis, defining the extracellular domain as a molecular ruler that keeps both membrane anchors at a certain distance. The coiled-coil contains a number of destabilizing residues at central heptad positions, which are conserved among all known tetherin sequences. Consequently, both the core of tetherin and the complete extracellular domain show a dramatic loss in thermostability upon disulfide bond reduction *in vitro*. Mutagenesis analyses reveal that the coiled-coil must be intact for function and identified an N-terminal conserved region that is required for HIV-1 restriction. The structure of tetherin explains how it can bridge long distances using a labile coiled coil motif and yet enough flexibility to insert with one membrane anchor into a budding virion while using the other anchor to remain excluded from the direct budding zone.

RESULTS

Recombinant tetherin forms dimmers

Recombinant tetherin(47–159) elutes from a SEC column at ~ 10.0 ml (Figure 1A); it migrates at ~ 13 kDa under reducing and at ~ 26 kDa under non-reducing conditions on SDS-PAGE indicating disulfide-linked dimerization (Figure 1B). Since crystals produced from tetherin(47–159) did not diffract beyond 10 Å resolution, we applied limited trypsin proteolysis to define a smaller fragment containing residues 80–147. Tetherin(80–147) elutes from a SEC column at ~ 11.3 ml (Figure 1A) and reveals disulfide-linked dimerization based on SDS-PAGE analysis under reducing and non-reducing conditions (Figure 1B). In order to test whether dimerization depends mainly on disulfide mediated cross-linking, both tetherin(47–159) and tetherin(80–147) were reduced with DTT and cysteines were subsequently blocked with iodoacetamide; this treatment produces mostly monomeric tetherin under non-reducing SDS-PAGE conditions (Figure 1C, lanes 1 and 2). Chemical cross-linking reveals that both constructs still dimerize as indicated by the appearance of new bands migrating at ~ 27 kDa (tetherin(47–159)) and between 15–20 kDa (tetherin(80–147)) (Figure 1C; lanes 4 and 6). Circular dichroism analyses show a high helical content (~ 90 % helical) for both constructs (Figure 2A). Although the helical content does not change for tetherin(47–159) in the presence of DTT, tetherin(80–147) displays a reduced helical content (~ 70%) (Figure 2A). The effect of the reducing agent was more dramatic when thermostability was tested. While tetherin(47–159) and tetherin(80–147) show melting temperatures (T_m) of ~61° C and ~57° C respectively, disulfide bond reduction drops the T_m to ~35° C and ~30° C, respectively (Figure 2B). The influence of disulfide bond linkage on the structure is further corroborated by the increased sensitivity of both constructs to complete degradation by trypsin treatment under reducing conditions (Figure S1). These results indicate that dimer stability greatly depends on intermolecular disulfide bonds.

Crystal structure of tetherin(80–147)

The crystal structure of tetherin(80–147) was determined from a selenomethionine-containing crystal using the single wavelength anomalous dispersion method and diffraction data to 2.77 Å resolution, which produced a readily interpretable electron density map (Figure 3A). The asymmetric crystal unit contained 11 monomers that together with crystallographic symmetry formed 6 identical dimers. The best defined dimer contains residues 89 to 147 and folds into a disulfide-linked 90Å long parallel coiled-coil (Figures 3B). The N-terminal residues 80–88 are disordered and the coiled-coil starts with Cys91 occupying the heptad d position followed by Val95 (a), Leu98 (d), and Leu102 (a). Glu105 (d) and the stutter at Gly109 splay the coiled-coil apart, documented by the increase in coiled-coil radius and pitch (Figure S2) beyond the regular coiled-coil features (Phillips, 1992). The following heptad positions Val113 (a) and Leu116 (d) still show an increased coiled-coil radius and pitch (Figure S2). More regular values are adopted along the heptad positions (Ile120(a), Leu123(d) and Leu127(a)) (Figure 3C). The irregularities which follow are produced by a stutter at Ala130, which tightens the coiled-coil radius to 4.3 Å (Figure S2), and Asn141 (d) that splays the coiled coil apart (Figure 3C and Figure S2). Despite these irregularities, the coiled-coil contains also stabilizing interactions such as salt bridges (Glu105 -Lys106, Glu133-Arg138) and an interhelical hydrogen bond (Asn141) (Figure 3C). All heptad positions are conserved among the known tetherin sequences. Modifications in some sequences include an extra helical turn before Gly100 and/or a deletion of two helical turns determined by Ala130 (a position) and Val134 (d position) (Figure S3).

The N-terminal extracellular region of tetherin extends the rod-like structure

SEC analysis of tetherin(47–159) shows a larger hydrodynamic radius compared to tetherin(80–149) (Figure 1A). This is further confirmed by small angle X-ray scattering analysis (Figure 4A). Guinier evaluation reveals radii of gyration (Rg) of 47.5 Å for tetherin(47–159) and 31.9 Å for tetherin(80–149). Maximal protein dimensions (D_{max}) of 170 Å (tetherin(47–159)) and 110 Å (tetherin(80–147)) were calculated by the distance distribution function p(r) (Figure S4). The shapes of the tetherin dimers were determined *ab initio* and the reconstructed models fit the experimental data with the discrepancy χ of 1.1 and 1.5, respectively (Figure 4A). The solution structure of tetherin(80–147) shows an elongated rod with dimensions of 110 × 45 × 30 Å, consistent with the 90 Å length of the rod seen in the crystal (Figure 4B). Tetherin(47–159) is more elongated and produces a rod with dimensions of 150 × 60 × 45 Å, confirming that the N-terminal region extends the coiled-coil part (Figure 4C). Part of the N-terminus in the rod is slightly bent and its orientation might be determined by the flexible linkage of the N-terminus to the coiled-coil domain as indicated by the protease sensitivity of this region (Figure S1).

The coiled-coil and the N-terminal region of tetherin are required for HIV-1 retention

We next analyzed whether disruption of coiled-coil residues influences tetherin function during HIV-1 retention. Two sets of coiled-coil mutations were designed based on the crystal structure; set 1 (Cys91Gly, Val95Tyr, Leu98Lys, Leu102His) disrupts the N-terminal part of the coiled-coil and set 2 (Leu127Lys, Ala130Tyr, Val134Glu, Leu137Glu) disrupts the C-terminal region. Recombinant forms of both mutants, tetherin(47–159)_set1 and tetherin(47–159)_set2 are soluble and elute from a SEC column in peaks overlapping with that of wild-type tetherin(47–159), indicating that the mutations change the hydrodynamic radius of the proteins (Figure S5A). The mutant proteins migrate slightly slower on SDS-PAGE than wild-type and reveal reduced disulfide-linked dimerization as determined under non-reducing SDS-PAGE conditions (Figure S5B). Chemical cross-linking corroborates further that the mutations interfere with dimerization; the set1 mutant shows slightly reduced dimerformation, while set 2 mutant shows a more dramatic reduction in dimerization as judged by the ratio of monomer dimer bands on SDS-PAGE in comparison to wild-type tetherin(47–159) (Figure S5B). This indicates that disruption of the C-terminal coiled-coil leads to a reduced detection of disulfide-linked dimers *in vitro*, which is most likely due to a defect in dimerization as detected by chemical cross-linking. In contrast, the set1 mutant shows only dramatically reduced disulfide-linked dimerization, although Cys 53 and Cys 63 are intact and could suffice to form disulfide-linked dimers (Andrew et al., 2009; Perez-Caballero et al., 2009).

Both sets of mutations were introduced into full-length tetherin containing an internal extracellular HA-tag (tetherin(iHA)) for expression in 293T cells. This indicates that tetherin(iHA)_set1 and set2 mutants are expressed on the surface of 293T cells (Figure 5C and D); they show membrane-staining similar to that of wild-type tetherin (Neil et al., 2008) and tetherin(iHA), which appears to concentrate in patches on the plasma membrane (Figure 5B). However, expression of the full-length tetherin set1 and set 2 mutants (C-terminal HA-tag) in cells infected with Vpu-deficient HIV-1 demonstrates that both mutants are no longer able to prevent HIV-1 release as indicated by the detection of capsid (CA) in the cell culture supernatant at similar levels as the vector control. In contrast expression of wild-type tetherin completely blocks HIV-1 release as expected. (Figure 6A, left panel). This thus implies that proper coiled-coil formation is required for tetherin function. Both mutants do not affect intracellular processing of Gag and were expressed at similar levels (Figure 6B, middle and right panels).

Since the extracellular region comprising residues 48 to 71 is highly conserved between different species (Figure S3), we tested two more sets of mutations by replacing conserved charged and polar side chains. Set 3 contains changes within residues 47 to 58 (Lys47Ala, Asn49Gly, Glu51Ala, Arg54Ser, Asp55Ala, Arg58Ser) and set 4 within residues 62 to 73 (Glu62Ala, Arg64Ser, Asn65Ala, His59Ser, Gln71Ala, Gln72Ala, Glu73Ser)(Figure S3). Both mutants are soluble when expressed as tetherin(47–159) and elute from a SEC column at the same position as wild-type tetherin(47–159) (Figure S6A). Furthermore they form disulfide linked dimers that can be efficiently cross-linked (Figure S6B). Both mutations were then introduced into full-length tetherin(iHA) and expressed in 293T cells. This demonstrates that both sets (3 and 4) of tetherin(iHA) mutants are expressed at the plasma membrane (Figure 5E and F). Although expression of the full-length set 3 mutant reveals its activity in HIV-1 retention at a level comparable to wild-type (Figure 6B, left panel; lanes 2 and 3), expression of the set 4 mutant shows no retention activity (Figure 6B, left panel; lane 4). Cells from all experiments reveal similar patterns of intracellular Gag processing (Figure 6B; middle panel). However, the extensive posttranslational modification observed for wild-type tetherin expression in 293T cells, which generates a high molecular weight smear, is less characteristic in the case of the set4 mutant (Figure 6B; right panel, lane 4).

Since the set4 mutant includes mutagenesis of the glycosylation site at Asn65, we constructed a single mutant of the glycosylation site at Asn65, Asn65Gln, to test whether the loss of retention activity is due to reduced glycosylation. Although the Asn65Gln mutant shows a less complex expression pattern (Figure 6C, right panel, lane 3) similar to tetherin_set4, the retention of HIV-1 was only slightly affected. A small amount of virus could escape since CA was detected in the supernatant (Figure 6C, left panel, lane 3). This indicates that the complete loss of retention observed for the set 4 mutant is most likely not due to the changes in post translational modification. Together our data indicate that a conserved N-terminal region of the extracellular domain is important for tetherin function.

Since the HA-tag of tetherin(iHA) was inserted into a flexible region (Figure S3) that is disordered in the crystal structure and sensitive to proteolysis (Figure S1), we tested the effect of the insertion on tetherin function. Expression of tetherin(iHA) reveals a slightly reduced HIV-1 retention activity in comparison to wild-type tetherin as judged by the detection of capsid (CA) in the supernatant (Figure 6D; left panel, lanes 2 and 3). Both wild-type and tetherin(iHA) show similar expression patterns (Figure 6D, right panel) and accumulation of intracellular Gag as compared to the vector control (Figure 6D, middle panel). This indicates that the conformational flexibility within residues 80 to 88 tolerates the insertion of the HA-tag but reduces the efficacy of HIV-1 retention slightly. Although we lack high resolution structural information of the N-terminus, the flexible region accommodating the HA-tag might correspond to the bent conformation of tetherin(47–159) observed in the model calculated based on SAXS data (Figure 4C).

DISCUSSION

Tetherin inhibits the release of some enveloped viruses including HIV-1 in the absence of Vpu (Neil et al., 2008) by bridging cellular and viral membranes (Perez-Caballero et al., 2009). Our structural analyses demonstrate that the complete extracellular domain of tetherin adopts an extended conformation that spans a maximal distance of 170 Å. More than halve of this is provided by a 90 Å-long parallel coiled-coil. The low resolution model based on X-ray scattering data indicates a slightly bent orientation of the N-terminal domain with respect to the coiled-coil. This might be due to flexibility within the region (residues 79 to 89) connecting the N-terminal and coiled-coil domains as documented by the sensitivity to proteolysis and the absence of an ordered structure for residues 80 to 88. In addition, this region permits the insertion of a HA-tag epitope without substantial loss of tetherin function.

The extracellular rod-like structure must be connected to the TMR via three N-terminal residues and to the GPI anchor via one C-terminal residue. Consequently it is unlikely that tetherin is positioned parallel between cellular and viral membranes which would tether virions quite close to the plasma membrane. The distance between both membranes would be less than 3 to 5 nm. Thin section electron microscopy images support a larger distance between virions and the plasma membrane (Neil et al., 2008; Perez-Caballero et al., 2009). Thus, upon virion tethering, the dimeric tetherin rod has most likely one end anchored in the plasma membrane and the other one in the virus membrane, as hypothesized (Perez-Caballero et al., 2009).

The length of the rod and its rather rigid structure in solution suggest that it functions as a molecular ruler that connects two entities via a 170 Å distance. The importance of the spacer function is documented by our mutagenesis studies of the coiled-coil region that abrogate HIV-1 retention and by the loss of function upon deletion of the coiled-coil (Perez-Caballero et al., 2009). Such a molecular ruler function might be also required to connect adjacent lipid rafts within the plasma membrane (Kupzig et al., 2003).

Single cysteine mutations do not affect tetherin function dramatically, but mutagenesis of all three cysteines lead to a complete loss of function during HIV-1 release (Andrew et al., 2009; Perez-Caballero et al., 2009) although the mutant is still active during Lassa and Marburg virus VLP release (Sakuma et al., 2009b). We show that the presence of disulfide bonds is crucial for the stability of the extracellular domain, since the melting temperature drops to 35°C (tetherin(47–159)) under reducing conditions. The low stability of tetherin under reducing conditions is most likely due to instability of the coiled-coil, which shows an even lower T_m under reducing conditions. The coiled-coil contains a number of coiled-coil destabilizing residues occupying central heptad positions. These positions do not follow classical knobs into holes packing but instead loosen the coiled-coil pitch and induce an expansion of its radius. Although the coiled-coil region contains two inter-helical salt bridges and one inter-helical hydrogen bond, which are employed to stabilize coiled-coils (Burkhard et al., 2002), the solvent exposure of the apolar heptad positions (Li et al., 2003) might contribute to the dramatic instability of the coiled-coil in the absence of the disulfide bond. Together these structural features explain the low T_m in the absence of stabilizing disulfide bonds.

This mode of labile coiled-coil interactions might serve two functions. First, tetherin's cellular function might involve the formation of heterodimers with a yet unknown ligand employing its coiled-coil to form more stable dimers. Secondly, the weak coiled-coil interactions together with the stabilizing disulfide bonds generate a dynamic structure, which permits disassembly and reassembly of the coiled-coil during dynamic processes. The latter function is in agreement with the presence of similar dynamic or destabilizing coiled-coil features in myosin (Blankenfeldt et al., 2006; Li et al., 2003), tropomyosin (Brown et al., 2001) and the streptococcus M1 protein (McNamara et al., 2008) that have been suggested to be important for their mode of action.

Despite its instability *in vitro*, we demonstrate the importance of the coiled-coil *in vivo*. Mutagenesis of N- and C-terminal sets of highly conserved heptad positions eliminates the tethering function, although the mutant proteins are still expressed on the plasma membrane. This indicates that the spacer function provided by proper coiled-coil formation is essential for tethering. We also identified a third set of residues within the highly conserved N-terminal extracellular region that are functionally required. Mutations within the stretch of residues 48 to 59 have no effect on tethering, whereas changes within residues 62 to 73 lead to a loss of the tethering function. Again both mutant proteins are expressed on the plasma membrane and the extracellular domains form dimers *in vitro*. Since the set 4 mutant

eliminates the glycosylation site at Asn65 and shows a less complex expression pattern as wild-type tetherin, we tested whether changes in posttranslational modification are responsible for loss of tetherin function. Although the expression pattern of Asn65Gln resembles that of the set 4 mutant, it only shows slightly reduced HIV-1 retention activity, consistent with previous findings reporting no effect on HIV-1 retention of single and double glycoslylation mutants of tetherin (Andrew et al., 2009). This indicates that mutagenesis of this N-terminal region (set 4) either affects its spacer function or eliminates an important docking site, possibly for self-assembly. Although Perez-Caballero reported that the N-terminus can be replaced by a similar region derived from the transferrin receptor and the coiled-coil can be replaced by the dystrophia myotonica protein kinase coiled-coil, it is important to note that the activity of art-tetherin is ~10-fold lower (Perez-Caballero et al., 2009). In contrast our data clearly demonstrate that the N-terminal domain and the dynamic features of the coiled-coil of tetherin are essential for HIV-1 retention.

Based on our structural analysis we propose the following interplay between the elongated shape and the conformational flexibility of tetherin. Although we do not know at which stage of assembly tetherin enters the virion membrane, it is likely that it is present from the beginning of assembly starting from lipid rafts. Since virus assembly and budding presents a dynamic process, tetherin cannot remain too rigid. The coiled-coil instabilities thus permit a certain degree of flexibility for the tetherin dimers to diffuse laterally into the budding site with four membrane anchors, while maintaining the strict distance between the membrane anchors. The conformational flexibility, which entails most likely opening and reassembly of the coiled-coil, is facilitated by the presence of the disulfide bonds. Consequently dimer dissociation and re-stabilization do not interfere with the dynamic process of virus assembly and budding while remaining anchored in the newly formed viral membrane and maintaining its spacer function. Furthermore the elongated rod-like structure might be involved in self-assembly as supported by the punctuate appearance of tetherin in the plasma membrane. Such clustering might require an intact N-terminal region, which could cluster tetherin around the membrane neck of a budding virion, consistent with the accumulation of tetherin at HIV-1 budding sites (Habermann et al., 2010). This would ensure that at least one or several tetherin dimers can efficiently insert into the viral membrane to render the system efficient.

EXPERIMENTAL PROCEDURES

Bacterial protein expression and purification

cDNA encoding human tetherin/BST-2 residues 47 to 159 and 80 to 147 were cloned into expression vector pETM11. Site directed mutagenesis of tetherin(47–159) was carried out using standard protocols and verified by sequencing. Protein expression was performed in *E. coli* Rosetta2 cells induced with IPTG at 20°C for 4 hours. Cells were lysed in buffer A (20mM Tris pH 8.0, 0.1M NaCl, 10mM imidazole) and proteins were purified by Ni^{2+} -chromatography. The His-tag was removed by TEV protease cleavage and both TEV and uncleaved protein were removed by Ni^{2+} -chromatography. Final purification steps included anion-exchange chromatography (mono Q; GE Healthcare) in buffer B (20 mM bicine pH 9.3, 0.1 M NaCl, 5 mM EDTA) and size-exclusion chromatography (Superdex 75; GE Healthcare) in buffer C (20 mM HEPES pH 8.0, 0.1 M NaCl, 5 mM EDTA). Selenomethionine substituted tetherin(80–147) and mutant tetherin proteins were purified as described above. Mutant tetherin constructs contain the following mutations: tetherin_set1, Cys91Gly, Val95Tyr, Leu98Lys, Leu102His; tetherin_set2, Leu127Lys, Ala130Tyr, Val134Glu, Leu137Glu; tetherin_set3, Lys47Ala, Asn49Gly, Glu51Ala, Arg54Ser, Asp55Ala, Arg58Ser; tetherin_set4, Glu62Ala, Arg64Ser, Asn65Ala, His59Ser, Gln71Ala, Gln72Ala, Glu73Ser.

Crystallization, data collection and structure solution

Tetherin(80–147) was crystallized at a concentration of 5 mg/ml by mixing 1 µl protein and 1 µl reservoir solution (0.02M $MgCl_2$, 0.1M bis tris pH5.0, 20% polyacrylic acid) at 20 °C. Crystals were cryo-protected in reservoir solution supplemented by 26% glycerol and flash-frozen in liquid nitrogen. A SAD dataset was collected at ESRF (Grenoble), beam line ID14-4. Data was indexed and processed with XDS (Kabsch, 1993) and scaled with SCALA (CCP4, 1994; Evans, 2006). The crystals belong to space group C2 with unit cell dimensions of a=169.89Å, b=85.93Å, c=123.31Å, β =126.94° and contain 11 monomers per asymmetric unit.

Heavy atom positions were located with SHELXD (Schneider and Sheldrick, 2002) and the correct hand was verified using SHELXE (Sheldrick, 2002). The experimental phases were calculated using SHARP (Bricogne et al., 2003) and resulted in an overall figure of merit (FOM) of 0.38/0.10 for the acentric and centric reflections respectively. These phases were improved using a 70% solvent content in SOLOMON (Abrahams and Leslie, 1996). An initial model was built using RESOLVE (Terwilliger and Berendzen, 1999), which allowed the determination of the non-crystallographic symmetry operators. The electron density map was further improved using 11-fold averaging and the final model was build manually using the program COOT (Emsley and Cowtan, 2004). The structure was refined to a resolution of 2.77 Å with the program PHENIX (Adams et al., 2002) with an Rf_{ac}tor of 0.24 and Rfr_{ee} of 0.27 with good stereochemistry (table 1). 96.88 % of the residues are within the preferred and allowed regions of a Ramachandran plot (CCP4, 1994). Chains A, F, I and J contain amino acids (aa) 89–147; chain B aa 89–145, chain C aa 89–137, chain D aa 87–142, chain E aa 88–146, chain G aa 88–141, chain H aa 89–142 and chain K aa 89–127. Molecular graphics figures were generated with PyMOL (http://www.pymol.org). The helical parameters of the coiled-coil were calculated using the program TWISTER (Strelkov and Burkhard, 2002). Coordinates and structure factors have been deposited in the protein data bank with accession number 2×7a.

Biophysical and biochemical characterization of tetherin

CD spectroscopy measurements were performed using a JASCO spectropolarimeter equipped with a thermoelectric temperature controller. Spectra of each sample were recorded at 20 °C in buffer D (20 mM phosphate, pH 7, 100 mM NaCl). For thermal denaturation experiments, the ellipticity was recorded at 222 nm with 1 °C steps from 20 to 100 °C with a slope of 1°/min. Ellipticity values were converted to mean residue ellipticity.

Proteolysis of tetherin was carried out in buffer C at room temperature with a trypsin to protein ratio of 1:100 (w/w). Dimerization of tetherin under reducing conditions was tested as follows. Proteins were reduced with 10 mM DTT and subsequently incubated with 100 mM iodoacetamide at room temperature for 1 hour. Unbound DTT and iodoacetamide were removed by dialysis in buffer C and samples were cross-linked with 5 mM EGS. The cross-linking reaction was quenched with 20 mM Tris pH 8.0.

Small angle X-ray scattering analysis

X-ray scattering data were collected on ESRF (Grenoble) beam line ID14-EH3 at a sample - detector distance of 2.4 m covering a range of momentum transfer of $0.1 < s < 4.5$ nm^{-1} ($s = 4\pi \sin(\theta)/\lambda$, where θ is the scattering angle and λ = 0.15 nm is the X-ray wavelength). The scattering intensity of tetherin(47–159) was measured at protein concentrations of 2 and 13 mg/ml and that of tetherin(80–147) at concentrations of 2 and 11 mg/ml in buffer C. The data were normalized to the intensity of the incident beam; the scattering of the buffer was subtracted and the resulting intensities were scaled for concentration. Data processing was performed using the program package PRIMUS (Konarev et al., 2003). The forward

scattering *I(0)* and the radius of gyration *Rg* were calculated with GNOM, which also provides the distance distribution function *p(r)* of the particle (Svergun, 1992). Low-resolution models of both tetherin samples were simulated by the program DAMMIN (Svergun, 1999) and GASBOR (Svergun et al., 2001), which resulted in similar elongated structures. Figure 4 represents the GASBOR model. The crystal structure of tetherin(80–147) was docked into the low resolution models using the program package SITUS (Wriggers et al., 1999).

Mammalian expression constructs and HIV-1 release assay

The coding sequence for full-length human tetherin with an N-terminal HA-tag (HA-tetherin) or an HA-tag inserted into the extracellular domain between residues Gln82 and Asp83 (tetherin(iHA)) was cloned into the mammalian expression vector pBJ5. To examine the effects of WT and mutant tetherin on HIV-1 release, 293T cells (1.2×10^6) were seeded into T25 flasks and transfected 24 hr later using a calcium phosphate precipitation technique. The cultures were transfected with 1 μg vpu-negative proviral DNA ($HIV\text{-}1_{HXB2}$) together with expression vectors for WT or mutant HA-tetherin, or the empty vector (50 ng). The total amount of transfected DNA was brought to 8 μg with carrier DNA (pTZ18U). Twenty-four h post transfection, the cells were lysed in radioimmunoprecipitation assay buffer (140 mM NaCl, 8 mM Na_2HPO_4, 2 mM NaH_2PO_4, 1% NP-40, 0.5% sodium deoxycholate, 0.05% SDS), and the culture supernatants were clarified by low speed centrifugation and passaged through 0.45-μm filters. Virions released into the medium were pelleted through 20% sucrose cushions by ultracentrifugation for 2 h at 27,000 rpm and 4°C in a Beckman SW41 rotor. Pelletable material and the cell lysates were analyzed by SDS-PAGE and Western blotting, using the anti-HIV CA antibody 183-H12-5C (Chesebro et al., 1992) to detect Gag proteins. HA-tagged tetherin was detected with the anti-HA mouse monoclonal antibody HA.11

Immunofluorescence analysis

Tetherin expression vectors containing the extracellular internal HA-tag were transfected into 293T cells using standard methods. For indirect immunofluorescence (IIF) 293T cells were cultured on coverslips and fixed with 4% paraformaldehyde for 20 min at 4°C. The cover slips were incubated with an αHA-tag antibody in PBS for 1h, at RT. Slides were washed three times with PBS, followed by the secondary antibody incubation at RT for 1h (Alexa488 or 594 coupled anti-mouse or anti-rabbit goat antibodies in in PBS). After three washes with PBS, slides were mounted in Mowiol and analyzed by confocal microscopy.

Supplementary Material

Refer to Web version on PubMed Central for supplementary material.

Acknowledgments

This work was supported by the Agence Nationale de la Recherche (ANR-08-BLAN-0271-01; WW) and the DFG SPP1175 (WW), the National Institute of Allergy and Infectious Diseases (R37AI029873 to HG) and a postdoctoral fellowship from the European Molecular Biology Organization (BH). We thank S. Avilov for help with confocal micrsocopy and B. Conell for characterization of the first tetherin constructs. We acknowledge the Partnership for Structural Biology (PSB; http://www.psb-grenoble.eu) for access to the common platforms including the crystallization facility (J. Marquez) and the ESRF and EMBL for beam time and assistance during data collection. The following reagent was obtained through the AIDS Research and Reference Reagent Program, Division of AIDS, NIAID, NIH: HIV-1 p24 monoclonal antibody (183-H12-5C) from Dr. Bruce Chesebro and Kathy Wehrly.

REFERENCES

Abrahams JP, Leslie AWG. Methods used in the structure determination of bovine mitochondrial F1 ATPase. Acta Cryst 1996;D52:30–42.

Adams PD, Grosse-Kunstleve RW, Hung L-W, Loerger TR, McCoy AJ, Moriarty NW, Read RJ, Sacchettini JC, Sauter NK, Terwilliger TC. PHENIX: building new software for automated crystallographic structure determination. Acta Cryst 2002;D58:1948–1954.

Andrew A, Miyagi E, Kao S, Strebel K. The formation of cysteine-linked dimers of BST-2/tetherin is important for inhibition of HIV-1 virus release but not for sensitivity to Vpu. Retrovirology 2009;6:80. [PubMed: 19737401]

Bartee E, McCormack A, Fruh K. Quantitative membrane proteomics reveals new cellular targets of viral immune modulators. PLoS Pathog 2006;2:e107. [PubMed: 17238276]

Blankenfeldt W, Thoma NH, Wray JS, Gautel M, Schlichting I. Crystal structures of human cardiac beta-myosin II S2-Delta provide insight into the functional role of the S2 subfragment. Proc Natl Acad Sci U S A 2006;103:17713–17717. [PubMed: 17095604]

Bricogne G, Vonrhein C, Flensburg C, Schiltz M, Paciorek W. Generation, representation and flow of phase information in structure determination: recent developments in and around SHARP 2.0. Acta Cryst 2003;D59:2023–2030.

Brown JH, Kim KH, Jun G, Greenfield NJ, Dominguez R, Volkmann N, Hitchcock-DeGregori SE, Cohen C. Deciphering the design of the tropomyosin molecule. Proc Natl Acad Sci U S A 2001;98:8496–8501. [PubMed: 11438684]

Burkhard P, Ivaninskii S, Lustig A. Improving coiled-coil stability by optimizing ionic interactions. J Mol Biol 2002;318:901–910. [PubMed: 12054832]

CCP4. The CCP4 suite: programs for protein crystallography. Acta Crystallogr D Biol Crystallogr 1994;50:157–163.

Chesebro B, Wehrly K, Nishio J, Perryman S. Macrophage-tropic human immunodeficiency virus isolates from different patients exhibit unusual V3 envelope sequence homogeneity in comparison with T-cell-tropic isolates: definition of critical amino acids involved in cell tropism. J Virol 1992;66:6547–6554. [PubMed: 1404602]

Douglas JL, Viswanathan K, McCarroll MN, Gustin JK, Fruh K, Moses AV. Vpu directs the degradation of the human immunodeficiency virus restriction factor BST-2/Tetherin via a {beta}TrCP-dependent mechanism. J Virol 2009;83:7931–7947. [PubMed: 19515779]

Emsley P, Cowtan K. Coot: model-building tools for molecular graphics. Acta Crystallographica Section D 2004;60:2126–2132.

Evans P. Scaling and assessment of data quality. Acta Crystallogr D Biol Crystallogr 2006;62:72–82. [PubMed: 16369096]

Goffinet C, Allespach I, Homann S, Tervo HM, Habermann A, Rupp D, Oberbremer L, Kern C, Tibroni N, Welsch S, et al. HIV-1 antagonism of CD317 is species specific and involves Vpu-mediated proteasomal degradation of the restriction factor. Cell Host Microbe 2009;5:285–297. [PubMed: 19286137]

Goto T, Kennel SJ, Abe M, Takishita M, Kosaka M, Solomon A, Saito S. A novel membrane antigen selectively expressed on terminally differentiated human B cells. Blood 1994;84:1922–1930. [PubMed: 8080996]

Gottlinger HG, Dorfman T, Cohen EA, Haseltine WA. Vpu protein of human immunodeficiency virus type 1 enhances the release of capsids produced by gag gene constructs of widely divergent retroviruses. Proc Natl Acad Sci U S A 1993;90:7381–7385. [PubMed: 8346259]

Gramberg T, Sunseri N, Landau NR. Accessories to the crime: recent advances in HIV accessory protein biology. Curr HIV/AIDS Rep 2009;6:36–42. [PubMed: 19149995]

Gupta RK, Hue S, Schaller T, Verschoor E, Pillay D, Towers GJ. Mutation of a single residue renders human tetherin resistant to HIV-1 Vpu-mediated depletion. PLoS Pathog 2009;5:e1000443. [PubMed: 19461879]

Habermann A, Krijnse Locker J, Oberwinkler H, Eckhardt M, Homann S, Andrew A, Strebel K, Kräusslich H-G. CD317/Tetherin is enriched in the HIV-1 envelope 1 and downregulated from the plasma membrane upon virus infection. J Virol. 2010 in press.

Harila K, Salminen A, Prior I, Hinkula J, Suomalainen M. The Vpu-regulated endocytosis of HIV-1 Gag is clathrin-independent. Virology 2007;369:299–308. [PubMed: 17822732]

Jia B, Serra-Moreno R, Neidermyer W, Rahmberg A, Mackey J, Fofana IB, Johnson WE, Westmoreland S, Evans DT. Species-specific activity of SIV Nef and HIV-1 Vpu in overcoming restriction by tetherin/BST2. PLoS Pathog 2009;5:e1000429. [PubMed: 19436700]

Jouvenet N, Neil SJ, Zhadina M, Zang T, Kratovac Z, Lee Y, McNatt M, Hatziioannou T, Bieniasz PD. Broad-spectrum inhibition of retroviral and filoviral particle release by tetherin. J Virol 2009;83:1837–1844. [PubMed: 19036818]

Kabsch W. Automatic processing of rotation diffraction data from crystals of initially unknown symmetry and cell constants. J Appl Cryst 1993;26:795–800.

Kaletsky RL, Francica JR, Agrawal-Gamse C, Bates P. Tetherin-mediated restriction of filovirus budding is antagonized by the Ebola glycoprotein. Proc Natl Acad Sci U S A 2009;106:2886–2891. [PubMed: 19179289]

Kawai S, Azuma Y, Fujii E, Furugaki K, Ozaki S, Matsumoto T, Kosaka M, Yamada-Okabe H. Interferon-alpha enhances CD317 expression and the antitumor activity of anti-CD317 monoclonal antibody in renal cell carcinoma xenograft models. Cancer Sci 2008;99:2461–2466. [PubMed: 19032371]

Klimkait T, Strebel K, Hoggan MD, Martin MA, Orenstein JM. The human immunodeficiency virus type 1-specific protein vpu is required for efficient virus maturation and release. J Virol 1990;64:621–629. [PubMed: 2404139]

Konarev PV, Volkov VV, Sokolova AV, Koch MHJ, Svergun DI. PRIMUS- a Windows-PC based system for small-angle scattering data analysis. J Appl Crystallogr 2003;36:1277–1282.

Kupzig S, Korolchuk V, Rollason R, Sugden A, Wilde A, Banting G. Bst-2/HM1.24 is a raft-associated apical membrane protein with an unusual topology. Traffic 2003;4:694–709. [PubMed: 12956872]

Li Y, Brown JH, Reshetnikova L, Blazsek A, Farkas L, Nyitray L, Cohen C. Visualization of an unstable coiled coil from the scallop myosin rod. Nature 2003;424:341–345. [PubMed: 12867988]

Malim MH, Emerman M. HIV-1 accessory proteins--ensuring viral survival in a hostile environment. Cell Host Microbe 2008;3:388–398. [PubMed: 18541215]

Mangeat B, Gers-Huber G, Lehmann M, Zufferey M, Luban J, Piguet V. HIV-1 Vpu neutralizes the antiviral factor Tetherin/BST-2 by binding it and directing its beta-TrCP2-dependent degradation. PLoS Pathog 2009;5:e1000574. [PubMed: 19730691]

Masuyama N, Kuronita T, Tanaka R, Muto T, Hirota Y, Takigawa A, Fujita H, Aso Y, Amano J, Tanaka Y. HM1.24 is internalized from lipid rafts by clathrin-mediated endocytosis through interaction with alpha-adaptin. J Biol Chem 2009;284:15927–15941. [PubMed: 19359243]

McNamara C, Zinkernagel AS, Macheboeuf P, Cunningham MW, Nizet V, Ghosh P. Coiled-coil irregularities and instabilities in group A Streptococcus M1 are required for virulence. Science 2008;319:1405–1408. [PubMed: 18323455]

McNatt MW, Zang T, Hatziioannou T, Bartlett M, Fofana IB, Johnson WE, Neil SJ, Bieniasz PD. Species-specific activity of HIV-1 Vpu and positive selection of tetherin transmembrane domain variants. PLoS Pathog 2009;5:pe1000300.

Mitchell RS, Katsura C, Skasko MA, Fitzpatrick K, Lau D, Ruiz A, Stephens EB, Margottin-Goguet F, Benarous R, Guatelli JC. Vpu antagonizes BST-2-mediated restriction of HIV-1 release via beta-TrCP and endo-lysosomal trafficking. PLoS Pathog 2009;5:e1000450. [PubMed: 19478868]

Miyagi E, Andrew AJ, Kao S, Strebel K. Vpu enhances HIV-1 virus release in the absence of Bst-2 cell surface down-modulation and intracellular depletion. Proc Natl Acad Sci U S A 2009;106:2868–2873. [PubMed: 19196977]

Neil SJ, Sandrin V, Sundquist WI, Bieniasz PD. An interferon-alpha-induced tethering mechanism inhibits HIV-1 and Ebola virus particle release but is counteracted by the HIV-1 Vpu protein. Cell Host Microbe 2007;2:193–203. [PubMed: 18005734]

Neil SJ, Zang T, Bieniasz PD. Tetherin inhibits retrovirus release and is antagonized by HIV-1 Vpu. Nature 2008;451:425–430. [PubMed: 18200009]

Ohtomo T, Sugamata Y, Ozaki Y, Ono K, Yoshimura Y, Kawai S, Koishihara Y, Ozaki S, Kosaka M, Hirano T, Tsuchiya M. Molecular cloning and characterization of a surface antigen preferentially

overexpressed on multiple myeloma cells. Biochem Biophys Res Commun 1999;258:583–591. [PubMed: 10329429]

Perez-Caballero D, Zang T, Ebrahimi A, McNatt MW, Gregory DA, Johnson MC, Bieniasz PD. Tetherin inhibits HIV-1 release by directly tethering virions to cells. Cell 2009;139:499–511. [PubMed: 19879838]

Phillips GN. What is the pitch of the alpha-helical coiled coil? Proteins: Structure, Function, and Genetics 1992;14:425–429.

Rong L, Zhang J, Lu J, Pan Q, Lorgeoux RP, Aloysius C, Guo F, Liu SL, Wainberg MA, Liang C. The transmembrane domain of BST-2 determines its sensitivity to down-modulation by human immunodeficiency virus type 1 Vpu. J Virol 2009;83:7536–7546. [PubMed: 19474106]

Sakuma T, Noda T, Urata S, Kawaoka Y, Yasuda J. Inhibition of Lassa and Marburg virus production by tetherin. J Virol 2009a;83:2382–2385. [PubMed: 19091864]

Sakuma T, Sakurai A, Yasuda J. Dimerization of tetherin is not essential for its antiviral activity against Lassa and Marburg viruses. PLoS One 2009b;4:e6934. [PubMed: 19742323]

Sauter D, Schindler M, Specht A, Landford WN, Münch J, Kim K-A, Votteler J, Schubert U, Bibollet-Ruche F, Keele BF, et al. Tetherin-Driven Adaptation of Vpu and Nef Function and the Evolution of Pandemic and Nonpandemic HIV-1 Strains. Cell Host Microbe 2009;6:409–421. [PubMed: 19917496]

Schneider TR, Sheldrick GM. Substructure solution with SHELXD. Acta Crystallogr D Biol Crystallogr 2002;58:1772–1779. [PubMed: 12351820]

Sheldrick GM. Macromolecular phasing with SHELXE. Zeitschrift für Kristallographie 2002;217:644–650.

Strebel K, Klimkait T, Maldarelli F, Martin MA. Molecular and biochemical analyses of human immunodeficiency virus type 1 vpu protein. J Virol 1989;63:3784–3791. [PubMed: 2788224]

Strebel K, Luban J, Jeang KT. Human cellular restriction factors that target HIV-1 replication. BMC Med 2009;7:48. [PubMed: 19758442]

Strelkov SV, Burkhard P. Analysis of [alpha]-Helical Coiled Coils with the Program TWISTER Reveals a Structural Mechanism for Stutter Compensation. Journal of Structural Biology 2002;137:54–64. [PubMed: 12064933]

Svergun DI. Determination of the regularization parameter in indirect transform methods using perceptual criteria. J. Appl. Crystallogr 1992;25:495–503. J Appl Crystallogr 25, 495–503.

Svergun DI. Restoring low resolution structure of biological macromolecules from solution scattering using simulated annealing. Biophys J 1999;76:2879–2886. [PubMed: 10354416]

Svergun DI, Petoukhov MV, Koch MH. Determination of domain structure of proteins from X-ray solution scattering. Biophys J 2001;80:2946–2953. [PubMed: 11371467]

Terwilliger EF, Cohen EA, Lu YC, Sodroski JG, Haseltine WA. Functional role of human immunodeficiency virus type 1 vpu. Proc Natl Acad Sci U S A 1989;86:5163–5167. [PubMed: 2472639]

Terwilliger TC, Berendzen J. Automated MAD and MIR structure solution. Acta Crystallographica Section D 1999;55:849–861.

Van Damme N, Goff D, Katsura C, Jorgenson RL, Mitchell R, Johnson MC, Stephens EB, Guatelli J. The interferon-induced protein BST-2 restricts HIV-1 release and is downregulated from the cell surface by the viral Vpu protein. Cell Host Microbe 2008;3:245–252. [PubMed: 18342597]

Wriggers W, Milligan RA, McCammon JA. Situs: A Package for Docking Crystal Structures into Low-Resolution Maps from Electron Microscopy. Journal of Structural Biology 1999;125:185–195. [PubMed: 10222274]

Zhang F, Wilson SJ, Landford WC, Virgen B, Gregory D, Johnson MC, Munch J, Kirchhoff F, Bieniasz PD, Hatziioannou T. Nef proteins from simian immunodeficiency viruses are tetherin antagonists. Cell Host Microbe 2009;6:54–67. [PubMed: 19501037]

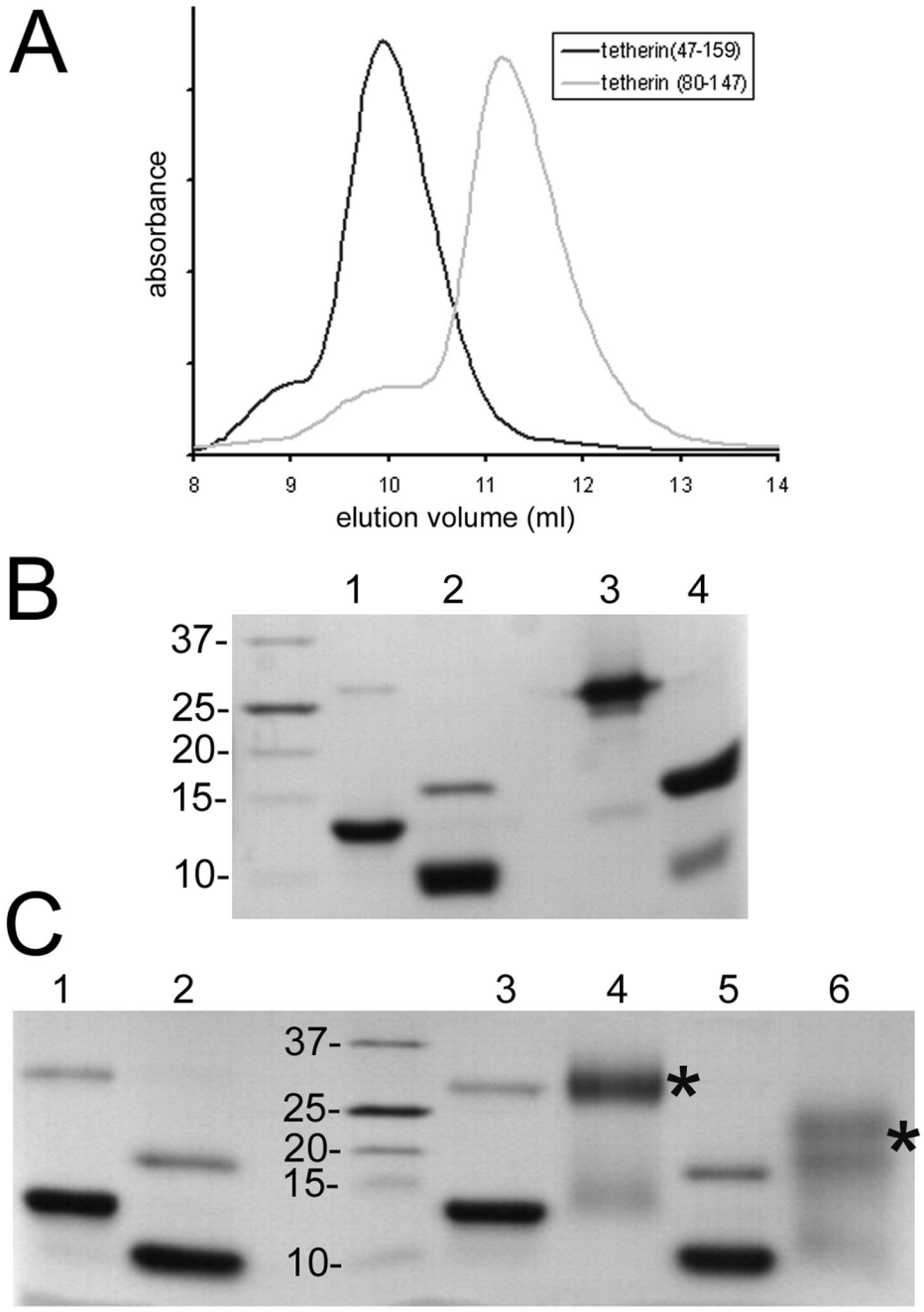

Figure 1. Biochemical characterization of the extracellular domain of tetherin

(A) SEC analysis of tetherin(47–159) and tetherin(80–147).

(B) SDS-PAGE of tetherin(47–159) (lanes 1 and 3) and tetherin(80–147) under reducing (lanes 1 and 2) and non-reducing conditions (lanes 3 and 4).

(C) Reduced tetherin(47–159) and tetherin(80–147) still dimerize; tetherin(47–159) (lanes 1, 3, 4) and tetherin(80–147) (lanes 2, 5, 6) were treated with iodoacetamide and separated under non-reducing conditions (lanes 1 and 2), under reducing conditions, lanes 3 and 5 and after cross-linking with 5 mM EGS (lanes 4 and 6); dimers are indicate by *.

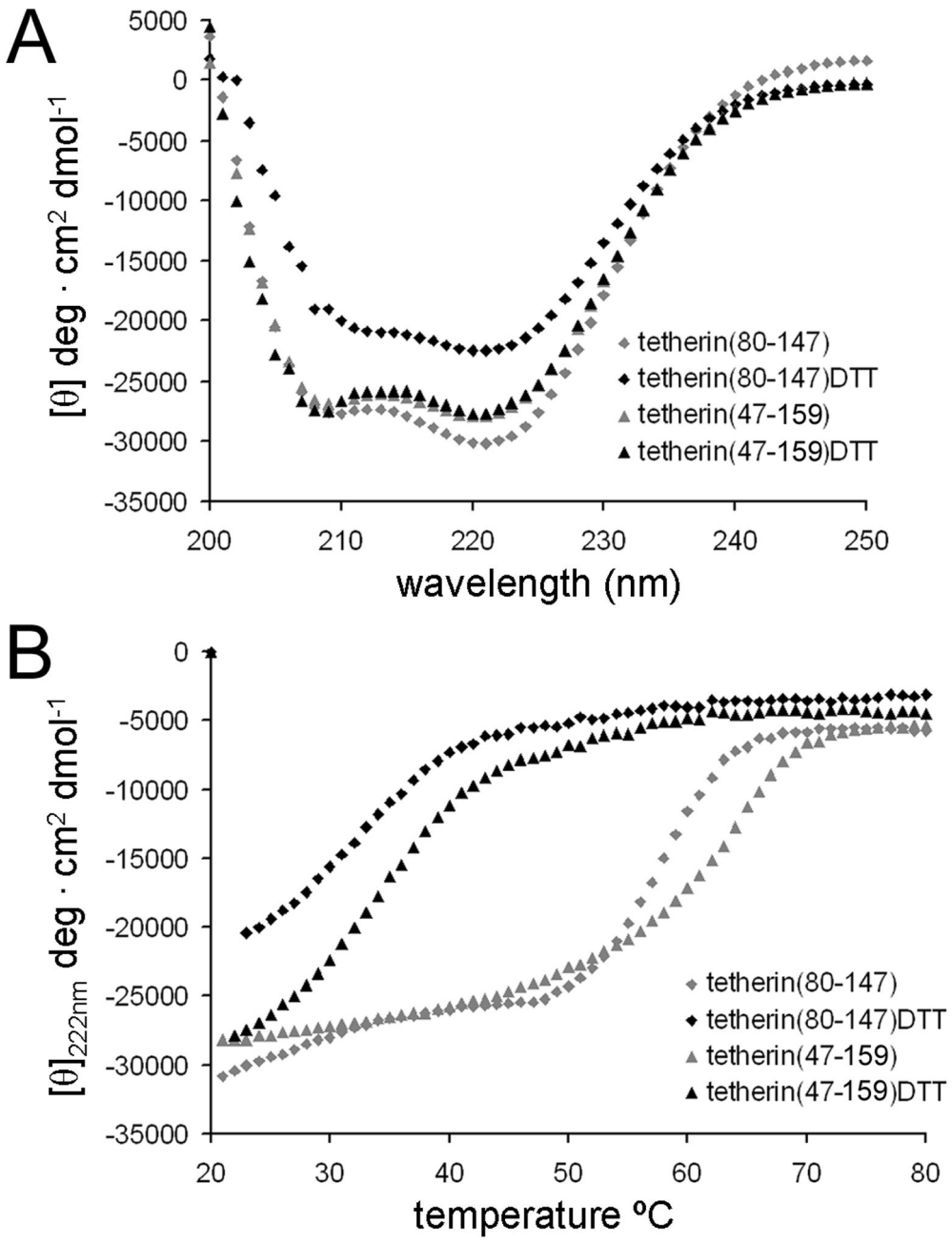

Figure 2. Disulfide bond reduction decreases the thermostability of tetherin

(A) Circular dichrosim analyses of tetherin under native and reducing conditions (DTT). Disulfide bond reduction of tetherin(80–147) reduces the overall helical content, while tetherin(47–159) is less affected.

(B) Thermostability measurements of tetherin were performed at 222 nm under native and reducing conditions (DTT), revealing a dramatic change in Tm after disulfide bond reduction.

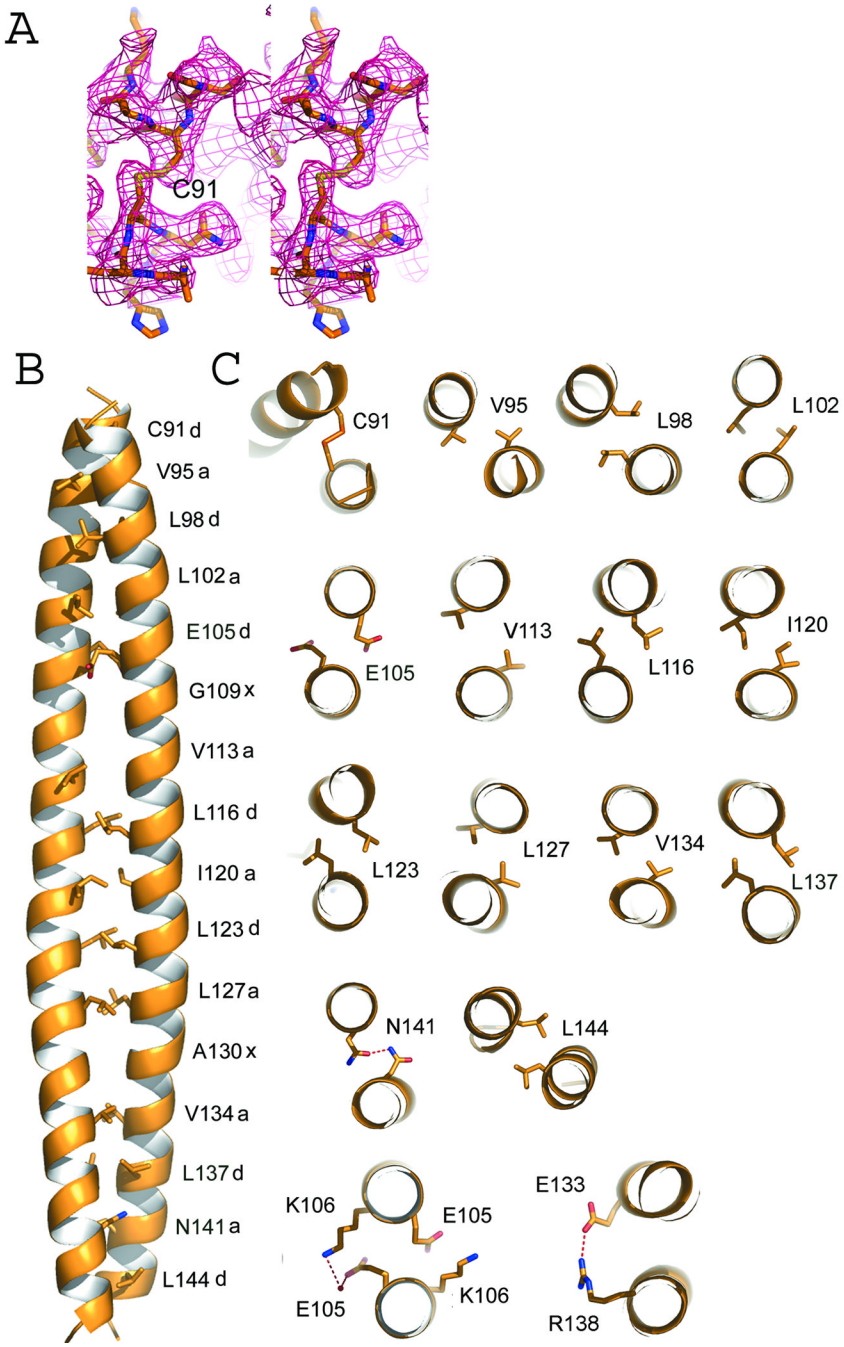

Figure 3. The crystal structure of tetherin(80–147)

(A) Stereo image of the experimental electron density map obtained after SAD phasing and non-crystallographic symmetry averaging; the heptad d position occupied by Cys91 forming a disulfide bond is shown.

(B) Ribbon representation shows a 90 Å long parallel coiled-coil.

(C) Close-up of the heptad motifs and polar dimerization contacts.

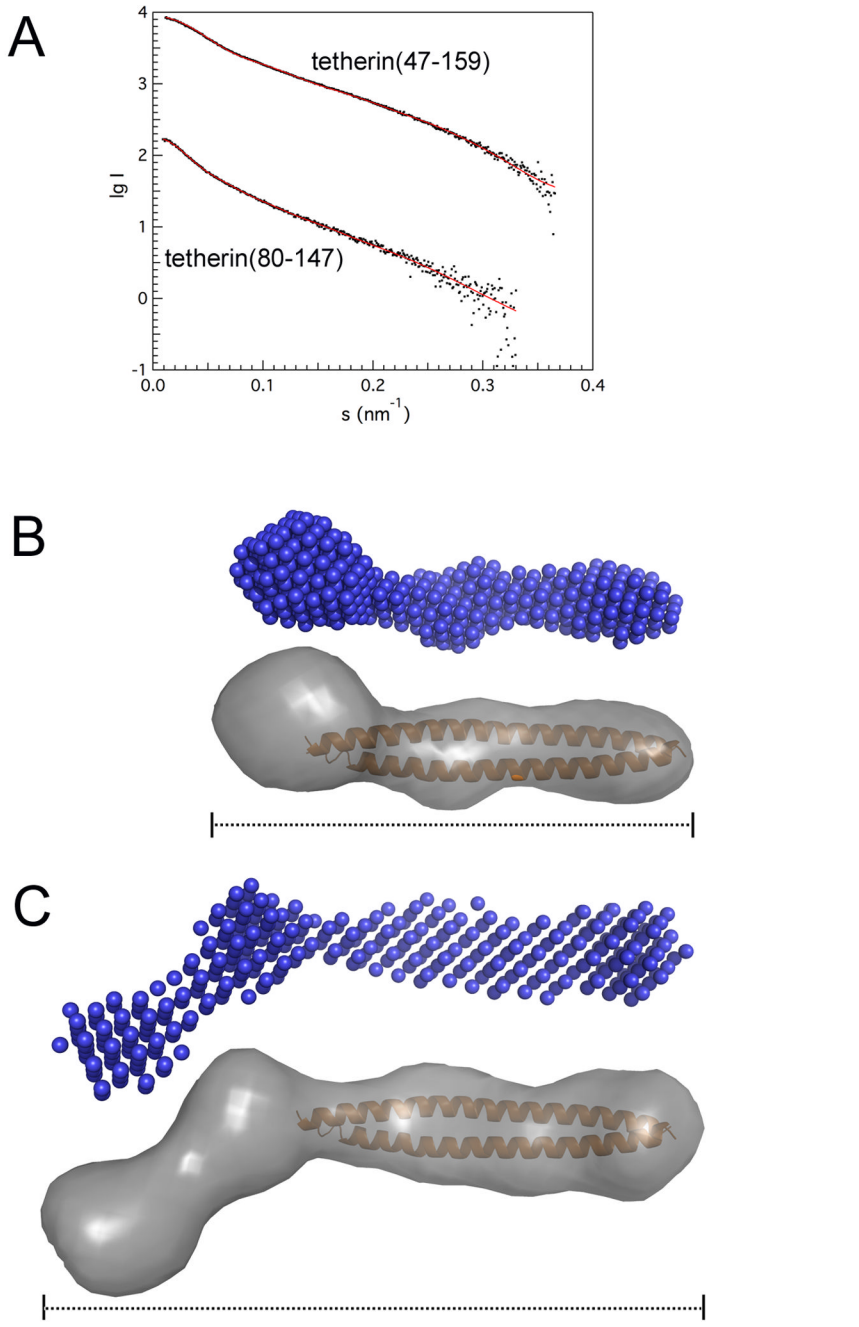

Figure 4. Small angle X-ray scattering analysis of tetherin

(a) Experimental scattering intensities obtained for tetherin(47–159) (upper curve) and tetherin(80–147) (lower curve) are shown as a function of resolution and after averaging and subtraction of solvent scattering. The scattering intensities calculated from representative models (presented in Figure 4B and C) with the lowest χ values are shown as red lines. The absolute values of the intensities of the upper curve are shifted by 2 logarithmic units. (B) *Ab initio* models of tetherin(80–147) and (C) of tetherin(47–159) reveal elongated rodlike structures; the calculated bead model as well as the molecular envelopes with the docked coiled-coil structure are shown.

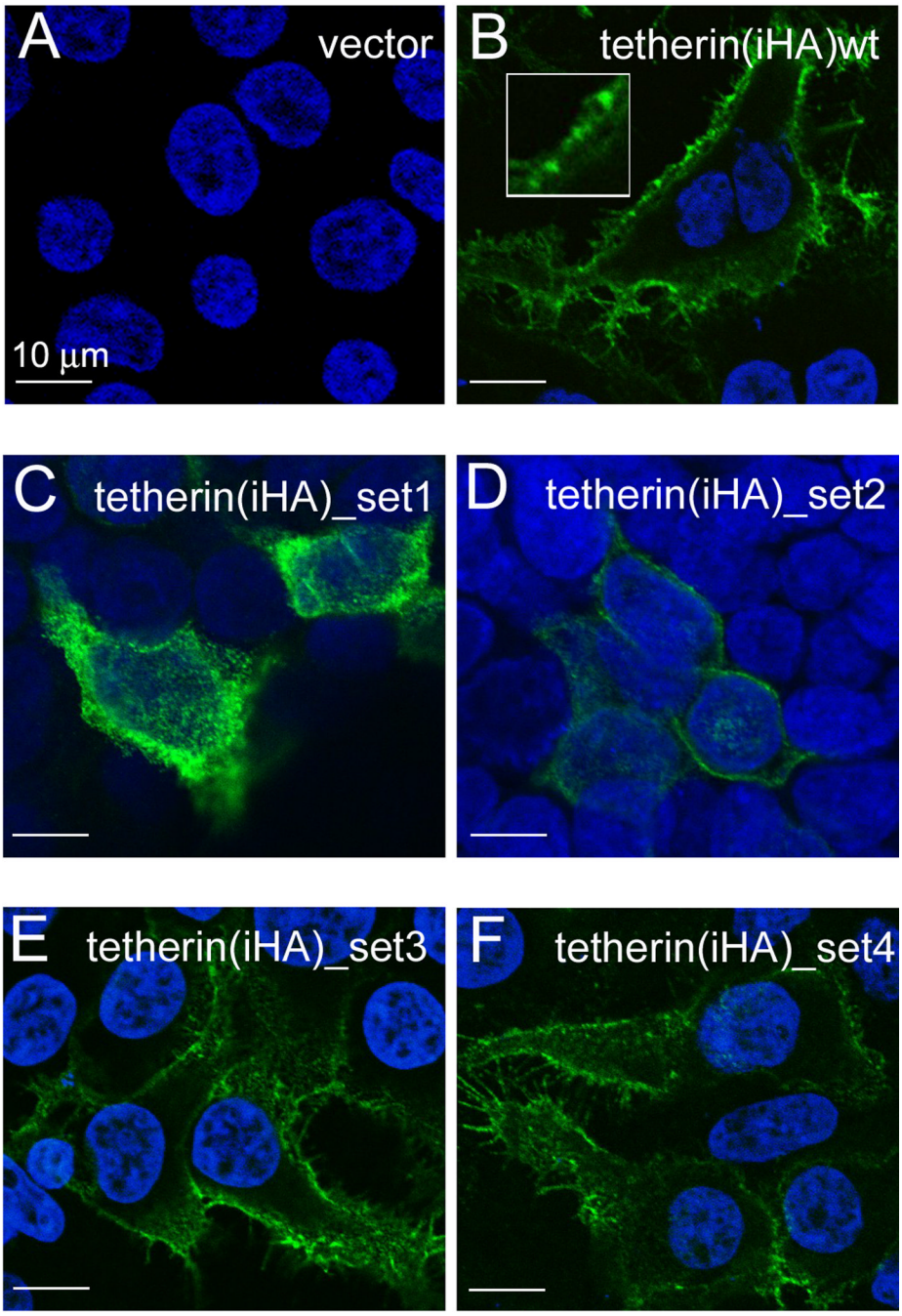

Figure 5. Cellular localization of wild type tetherin and mutants forms of tetherin

Immunofluorescence of (A) MOCK transfected 293T cells showing DAPI staining.
(B) tetherin(iHA); the inset shoes a close-up of a section of the plasma membrane revealing patches of tetherin staining.
(C) tetherin(iHA-set1)
(D) tetherin(iHA-set2)
(E) tetherin(iHA-set3)
(F) tetherin(iHA-set4); all constructs reveal a similar plasma membrane staining pattern, indicating that the mutations do not affect their localization.

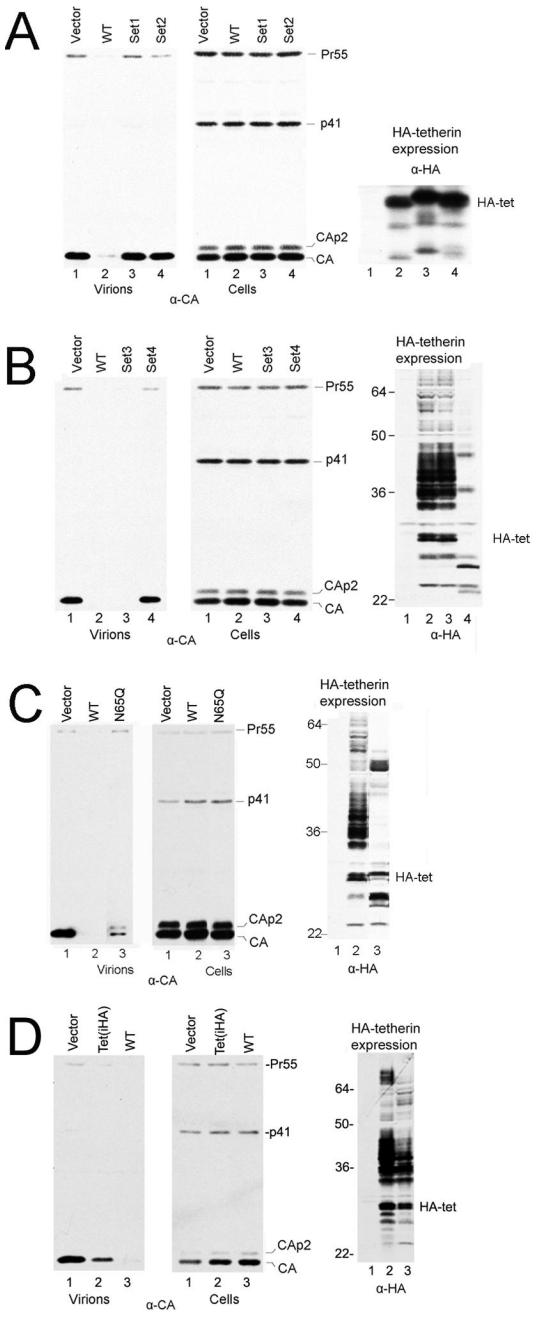

Figure 6. Mutations within the coiled-coil and the N-terminal region affect tetherin function during HIV-1 retention

(A) Expression of tetherin_set1 and tetherin_set2 abolish the retention function of tetherin. Release of virions (left panel, lanes 3 and 4) is the same as in case of the vector control (lane 1), whereas wild-type tetherin prevents virion release (left panel, lane 2). The middle panel shows that intracellular Gag and its processing are not affected by the expression of mutant tetherin (lanes 3 and 4). The right panel shows the expression levels of mutant (lanes 3 and 4) and wild type tetherin (lane 2).

(B) Expression of tetherin_set3 (left panel) has no effect on tetherin function (lane 3) while tetherin_set4 abolishes the retention function of tetherin (lane 4) as indicated by the

extracellular detection of CA. The middle panel shows that intracellular Gag and its processing are not affected by the expression of mutant tetherin (lanes 3 and 4). The right panel shows the expression levels of mutant and wild type tetherin. Note that the extensive posttranslational modification observed for wild type tetherin is absent in case of the set 4 mutant.

(C) Expression of the tetherin mutant Asn65Gln (N65Q)(left panel) has little effect on tetherin function (lane 3) compared to wild-type tetherin (lane 2). Intracellular Gag processing is not affected by the expression of the N65Q mutant (middle panel; lanes 2 and 3). The right panel shows that the expression pattern of N65Q (lane 3) is less complex than that of wild type tetherin (lane 2).

(D) Expression of tetherin(iHA) (left panel) has little effect on tetherin function (lane 2) when compared to wild-type tetherin (lane 3). The middle panel shows that intracellular Gag and its processing are not affected. The right panel shows the expression levels of tetherin(iHA) and wild-type tetherin.

Table 1

Crystallographic statistics

Data collection statistics	
Space group	C2
Cell dimensions a, b, c; β ;	169.89 Å, 85.93 Å, 123.31 Å; 126.94°
Wavelength (Å)	0.979
Resolution(Å)	45.00 - 2.77 (2.92 – 2.77)
R_{merge}	0.086 (0.479)
Completeness (%)	98.1 (97.7)
I/ σ(I)	13.8 (3.8)
Redundancy	7.6 (7.7)
Refinement statistics	
Resolution range (Å)	44.8-2.77
No reflections	35361
R_{work} / R_{free}	0.2407/0.2737
No protein atoms	4596
No of ligands/ion	21
No of waters	126
B-factors protein/ligand/water	88.56/62.65/66.31
R.m.s.d (bonds)(Å)	0.014
R.m.s.d (angles)(°)	1.305

Values in parentheses are for highest-resolution shell.